

ARTICLE

Received 31 May 2012 | Accepted 7 Dec 2012 | Published 22 Jan 2013

DOI: 10.1038/ncomms2369

Visualizing the atomic-scale electronic structure of the $\text{Ca}_2\text{CuO}_2\text{Cl}_2$ Mott insulator

Cun Ye^{1,*}, Peng Cai^{1,*}, Runze Yu², Xiaodong Zhou¹, Wei Ruan¹, Qingqing Liu², Changqing Jin² & Yayu Wang¹

Although the mechanism of superconductivity in the cuprates remains elusive, it is generally agreed that at the heart of the problem is the physics of doped Mott insulators. A crucial step for solving the high temperature superconductivity puzzle is to elucidate the electronic structure of the parent compound and the behaviour of doped charge carriers. Here we use scanning tunnelling microscopy to investigate the atomic-scale electronic structure of the $\text{Ca}_2\text{CuO}_2\text{Cl}_2$ parent Mott insulator of the cuprates. The full electronic spectrum across the Mott-Hubbard gap is uncovered for the first time, which reveals the particle-hole symmetric and spatially uniform Hubbard bands. Defect-induced charge carriers are found to create broad in-gap electronic states that are strongly localized in space. We show that the electronic structure of pristine Mott insulator is consistent with the Zhang-Rice singlet model, but the peculiar features of the doped electronic states require further investigations.

¹State Key Laboratory of Low Dimensional Quantum Physics, Department of Physics, Tsinghua University, Beijing 100084, China. ²Beijing National Laboratory for Condensed Matter Physics, Institute of Physics, Chinese Academy of Sciences, Beijing 100190, China. * These authors contributed equally to this work. Correspondence and requests for materials should be addressed to Y.W. (email: yayuwang@tsinghua.edu.cn).

Soon after the discovery of high T_C (critical temperature) superconductivity in the cuprates, it was realized that the superconducting phase lies in close proximity to an insulating state¹. The cuprate parent compound has one unpaired electron per Cu site, and is predicted by band theory to be a half-filled metal. The strong onsite Coulomb repulsion, however, prohibits electron hopping between neighbouring sites and leads to a Mott insulator ground state with antiferromagnetic (AF) ordering. Charge carriers doped into the CuO_2 plane destroy the insulating phase and superconductivity emerges as the carrier density is sufficiently high. The main challenge in the quest for understanding high T_C superconductivity is to describe the behaviour of the doped charge carriers in the presence of strong electron correlations². A natural starting point for tackling this formidable task is to elucidate the electronic structure of the parent Mott insulator, and see how a single electron or hole behaves in the AF spin background.

Despite extensive experimental studies on the parent and lightly doped Mott insulators, a comprehensive picture about their electronic structure is still lacking. Optical spectroscopy³ and resonant inelastic X-ray spectroscopy^{4,5} can probe the excitations across the Mott–Hubbard gap, but they cannot detect the ground-state electronic structure directly. Angle-resolved photoemission spectroscopy (ARPES) provides direct momentum (k) space structure of the occupied lower Hubbard band (LHB)^{6,7}, but is unable to reach the empty states above the Fermi level (E_F), leaving the upper Hubbard band (UHB) unexplored. The lack of complete spectroscopic information across the Mott–Hubbard gap makes it difficult to clarify how the high-energy spectral weight is transferred to the low-energy states near E_F , upon which superconductivity emerges.

Another vital piece of information that is still missing is the spatial characteristic of the Mott insulator electronic structure. As the Mott physics is dictated by onsite Coulomb repulsion, the real-space picture could be more relevant than the k -space picture, which has been extremely successful in describing weakly interacting electron systems. Especially, atomic-scale resolution becomes indispensable if we want to experimentally illustrate the electronic properties of a single charge doped into the AF background.

Scanning tunnelling microscopy (STM) is an ideal spectroscopic technique for filling the aforementioned gaps in our understanding of doped Mott insulators. STM can directly map out the electronic states, both below and above E_F , with the unique capability of atomic-scale spatial resolution. STM studies on high T_C cuprates have revealed a variety of remarkable phenomena, including the impurity resonance^{8,9}, checkerboard ordering^{10–13} and phase incoherent Cooper pairing^{14,15}. However, the parent Mott insulator phase has never been investigated by STM, most likely owing to the technical challenges associated with tunnelling into a good insulator.

Here, we report the first STM study of the atomic-scale electronic structure of the $\text{Ca}_2\text{CuO}_2\text{Cl}_2$ (CCOC) parent Mott insulator of the cuprates. The full electronic spectrum across the Mott–Hubbard gap is uncovered by tunnelling spectroscopy, which reveals the particle–hole symmetric and spatially uniform Hubbard bands. Defect-induced charge carriers are found to create broad in-gap electronic states that are strongly localized in space. The electronic structure of the pristine Mott insulator is in good agreement with the single-band Zhang–Rice singlet (ZRS) model, but the peculiar features of the doped electronic states require further investigations.

Results

Topographical properties of the CCOC surface. The oxychloride cuprate CCOC Mott insulator is chosen for its high crystal

quality and excellent cleavage properties. Figure 1a shows the schematic crystal structure of CCOC, which is similar to that of the prototypical parent compound La_2CuO_4 . The crystal cleaves easily between two adjacent CaCl layers, exposing the Cl terminated surface. The CuO_2 plane lies at 2.73 Å below the surface and the Cu sites are directly underneath the exposed apical Cl atoms. The local electronic properties of hole-doped $\text{Ca}_{2-x}\text{Na}_x\text{CuO}_2\text{Cl}_2$ have been extensively studied by STM^{13,16–18}. In this work, we report the first STM study of the pristine CCOC Mott insulator phase. Details about the sample growth and STM measurements are described in the Methods session and Supplementary Fig. S1.

Figure 1b displays a typical STM topography of cleaved CCOC taken at $T = 77$ K with sample bias $V_s = -3.5$ V and tunnelling current $I_t = 10$ pA, which reveals a large area of atomically flat terrace. The Cl atoms form a regular square lattice with lattice constant $a \sim 3.9$ Å, in agreement with the tetragonal unit cell of CCOC. The cross-shaped dark spots in the image correspond to the missing Cl defects (or Cl vacancies), which are created during the cleaving process. The inset of Fig. 2a displays the high-resolution STM image of a defect-free area, which has arguably the most ideal surface structure for the cuprates without the complications from structural supermodulations and electronic inhomogeneities.

Electronic structure of pristine CCOC. The local electronic structure of CCOC is probed by dI/dV (differential conductance) spectroscopy, which is approximately proportional to the electron density of state (DOS). Figure 2a displays the spatially averaged dI/dV curve obtained on the defect-free surface shown in the inset (the individual curves are displayed in the Supplementary Fig. S2). The full electronic spectrum across the Mott–Hubbard gap is directly uncovered for the first time. The occupied state dI/dV curve is very similar to the ARPES measured energy distribution curves of CCOC^{6,19}, especially those along the $(0, \pi)$ direction as discussed in Supplementary Fig. S3 and Supplementary Note 1. As the parent cuprate is a charge transfer insulator with oxygen bands lying between the LHBs and UHBs²⁰, the shoulder near $V_s = -0.8$ V is ascribed to the charge transfer band (CTB) and the rapid increase for $V_s < -1.5$ V is

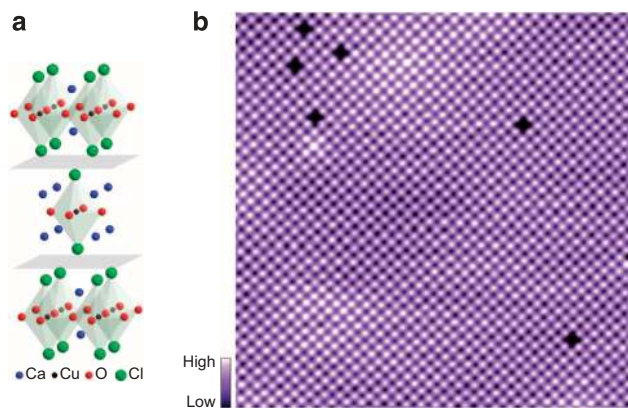


Figure 1 | Crystal structure and STM topography on CCOC. (a) Crystal structure of CCOC, which is similar to that of La_2CuO_4 except that the LaO layer is replaced by CaCl layer. The crystal cleaves easily between two adjacent CaCl layers, as indicated by the grey planes, exposing the square lattice of Cl atoms. (b) Constant current topographical image (155×155 Å) of CCOC taken at bias voltage $V_s = -3.5$ V and tunnelling current $I_t = 10$ pA. Each cross-shaped dark site on the surface corresponds to a missing Cl defect.

due to the non-bonding O $2p_{\pi}$ state^{6,19}. The totally new feature revealed by Fig. 2a is the UHB above E_F , which was an unexplored territory before this report. The simultaneous observation of CTB and UHB immediately reveals several key spectroscopic features of the Mott insulator. The effective Mott–Hubbard gap, or more precisely the charge transfer gap, can be directly measured to be $\Delta = 2.2$ eV. This value is very close to the 2.1 eV gap size obtained by optical reflectivity on parent CCOC³. The excellent agreement with the optical and ARPES results indicate that the tip-induced band bending, which may affect STM results on insulating materials, is negligible in our measurement. Shown in Fig. 2b are the zoom-in dI/dV curves of the CTB and UHB, which can fit well by using a broad Gaussian function rather than a sharper Lorentzian. Similar feature has been observed by previous ARPES measurements and interpreted as evidence for the breakdown of the coherent quasiparticle picture in Mott insulators¹⁹. The full-width at half-

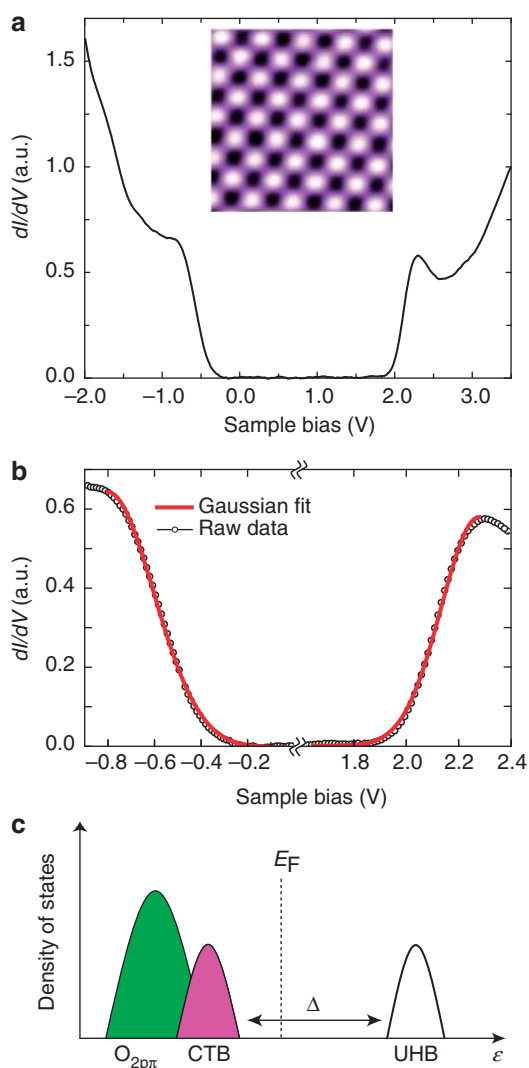


Figure 2 | Spectroscopy and electronic structure of pure CCOC.

(a) Spatially averaged dI/dV spectrum over a defect-free area of CCOC reveals the full electronic structure across the Mott gap. (Inset) High-resolution image ($28 \text{ \AA} \times 28 \text{ \AA}$) of the area where the spectra are taken. (b) Closed-up dI/dV curves of the charge transfer band (CTB) and the upper Hubbard band (UHB). The red curves show the Gaussian fit to the data. (c) Schematic band structure of the pristine Mott insulator showing the UHB (unfilled), the CTB (pink) and the non-bonding O $2p_{\pi}$ band (green).

maximum for the CTB and UHB are $\Gamma = 0.47$ and 0.34 eV, respectively, which are comparable to the bandwidth $W = 0.35$ eV determined by the ARPES measured band dispersion¹⁹. The similar lineshape, bandwidth and peak DOS value of the CTB and UHB spectra demonstrate the approximate particle–hole symmetry across the charge transfer gap of the Mott insulator. The electronic structure of the Mott insulator phase is schematically illustrated in Fig. 2c.

We next turn to the spatial distribution of the electronic structure, which is an issue of great importance to Mott insulator where the local Coulomb repulsion has a dominant role. As the lowest energy excitation of the charge transfer insulator is the removal of an electron from the occupied O $2p$ orbital to the unoccupied Cu $3d_{x^2-y^2}$ orbital²⁰, naively it is expected that the unpaired hole will mainly reside on the anion ligands and electron on the cation d orbitals²¹. This picture implies that the relative weight of CTB and UHB may vary between the Cu and O sites. However, our atomically resolved dI/dV spectroscopy shown in Fig. 3 reveals that the entire electronic structure is highly uniform in space without significant difference between the Cu, O and Ca sites. This observation suggests that both the CTB and UHB of parent cuprate form extended states in space rather than keeping their local orbital characteristics.

Electronic states of doped charges. Now that the electronic structure of pristine CCOC is well established, we are ready to investigate the electronic state created by an added charge. For this purpose, we take advantage of the defects that naturally occur in pristine CCOC. The most common defects on cleaved CCOC are the missing Cl atoms on the top surface, as revealed in Fig. 1b. As each Cl^- ion strongly grasps an extra electron, a missing Cl effectively donates an electron into the CuO_2 plane. The red curve in Fig. 4a shows the dI/dV measured directly on the missing Cl site (or the exposed Cu site of the underneath CuO_2 plane) compared with that taken at a location far from the defect (black curve). The most dramatic spectroscopic feature caused by the doped electron is the emergence of a broad electronic state within the charge transfer gap near the edge of the UHB. Meanwhile, the peak of the UHB is completely suppressed, indicating the transfer

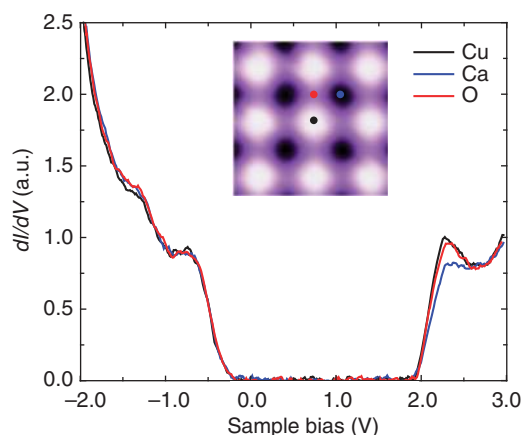


Figure 3 | Spatial distribution of the electronic structure in CCOC. The black, blue and red curves show the spatially resolved dI/dV spectra taken at the Cl (Cu), Ca and O sites of the CCOC surface, respectively. The setup conditions are $V_s = -3$ V and $I_t = 10$ pA. There is no significant difference between the spectra, demonstrating spatially uniform electronic structures. (Inset) Closed-up topography of the pure CCOC surface. The black, blue and red dots indicate the locations where the corresponding spectra are taken.

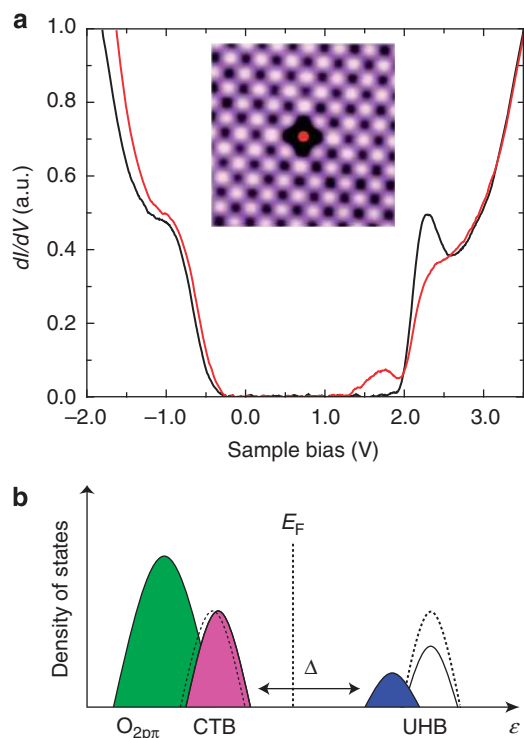


Figure 4 | Electronic structure of the missing Cl defect. (a) The red curve shows the dI/dV spectrum measured at the missing Cl defect centre and the black curve is taken at six lattice distances away from the defect. (Inset) High-resolution image ($35 \text{ \AA} \times 35 \text{ \AA}$) around a missing Cl defect and the red dot indicates where the red curve is taken. (b) Schematic electronic structure at the defect centre: an in-gap state (blue) emerges near the edge of UHB owing to spectral weight transfer from the latter. The CTB is slightly shifted and the local gap amplitude is significantly reduced.

of its spectral weight to the in-gap state. The CTB, in contrast, only shifts slightly, revealing a strong particle-hole asymmetry induced by the doped electron. As a consequence of the in-gap state, the local charge transfer gap at the defect centre is reduced to $\Delta = 1.6 \text{ eV}$. The schematic electronic structure induced by the doped electron is drawn in Fig. 4b.

The spatial distribution of the doped electronic state is another fundamental issue that STM is particularly suited for investigating. Figure 5a shows a series of dI/dV spectra taken as the STM tip is positioned away from the defect centre along the Cu-O bond direction (inset of Fig. 5a), which reveals the vanishing in-gap state accompanied by the emerging UHB peak. At a distance of six lattice constants from the defect centre, the dI/dV curve becomes similar to that of the pristine Mott insulator. By subtracting this background from the dI/dV curve at each location, the relative contribution of the defect state can be extracted. As shown in Fig. 5b, both the amplitude of the in-gap state and the suppression of UHB decrease systematically with increasing distance from the defect centre. Figure 5c shows that the profile can fit very well by using two Gaussian terms representing the created in-gap state and suppressed UHB, respectively (see Supplementary Fig. S4 for details). The spectral weight of the in-gap state can be roughly estimated by the area enclosed by the Gaussian fit (Supplementary Note 2). Figure 5d summarizes the spatial evolution of the spectral weight, which loses half of its strength within a distance of three lattice sites, or merely 12 \AA from the defect centre. The in-gap state is thus strongly localized in space, presumably owing to the frustrated motion of the doped charge in the AF background.

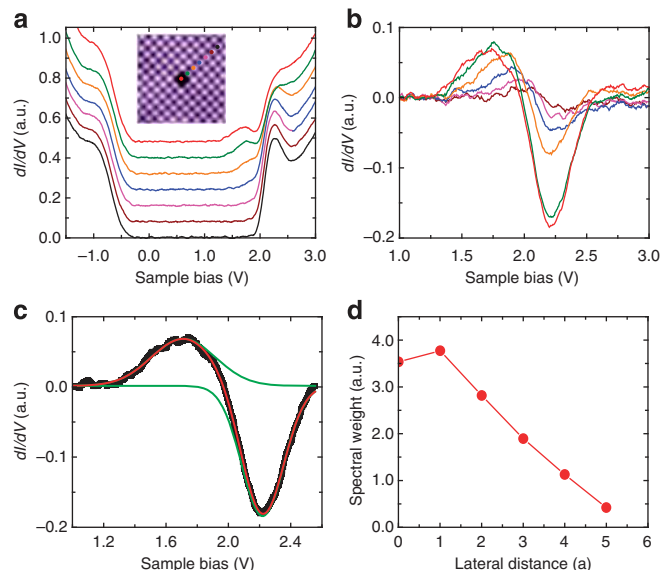


Figure 5 | Spatial distribution of the doped electronic state. (a) A series of dI/dV spectra taken at locations away from the missing Cl defect centre along the Cu-O bond direction, as indicated by the coloured dots. (b) Contribution of the doped electronic state to local electronic structure obtained by subtracting the background dI/dV (acquired at six lattice distances away from the defect) from each dI/dV spectrum in a. (c) The red curve in b can fit well by two Gaussian terms and the spectral weight of the in-gap state can be estimated by the area enclosed by the Gaussian lineshape. (d) Spatial dependence of the in-gap state spectral weight, which decays rapidly with increasing lateral distance from the defect centre.

Bias-dependent topography near the missing Cl defect reveals another highly unexpected feature. Figure 6a shows the STM image taken at negative bias $V_s = -3.0 \text{ V}$, which probes the occupied state. Except for the missing Cl atom, there is no other pronounced spatial feature. Figure 6b displays the image taken at the same area with positive bias $V_s = 3.5 \text{ V}$, which shows a dramatic spatial pattern where the four next-nearest-neighbour sites appear to be anomalously bright (illustrated in Fig. 6c). The bias-dependent images further demonstrate the particle-hole asymmetry induced by the doped electron. Interestingly, similar patterns have been seen at Ni impurity in superconducting $\text{Bi}_2\text{Sr}_2\text{CaCu}_2\text{O}_{8+\delta}$, where the next-nearest-neighbour sites brighten up in the positive-bias DOS map⁹. It will be intriguing to find out if the spatial pattern of a doped electron in the Mott insulator is related to that of the Ni impurity states in superconducting cuprates.

Besides the well-defined missing Cl defect on the surface, there exists another type of defect that occurs in the bulk of CCOC. Figure 6d,e show the topographical images around such a defect at negative and positive biases, respectively. The images exhibit totally different bias dependence as compared with that of the missing Cl defect. The four nearest-neighbour Cu sites around the defect centre become anomalously bright at negative bias, while at positive bias they are slightly suppressed. In both images, the surface Cl layer retains the perfect crystalline order, and the defect is located at the centre of the four-Cl plaquette in the underneath layer, which corresponds to the Ca site as illustrated in Fig. 6f.

Figure 7 displays the dI/dV spectra around the Ca-site defect at the locations marked by the dots in the inset. Right at the defect centre (the red curve), the spectrum also shows a broad in-gap state. It lies close to the lower edge of the charge transfer gap, rather than the upper gap edge as the missing Cl defect.

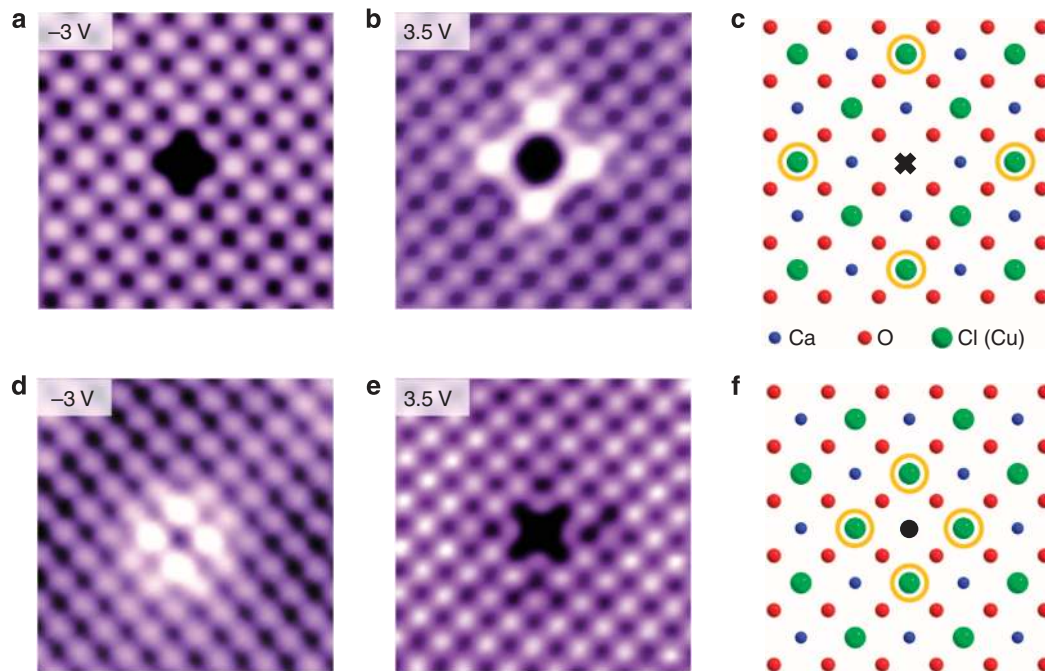


Figure 6 | Bias-dependent images around the defects. (a,b) Constant current images ($35 \text{ \AA} \times 35 \text{ \AA}$) around a missing Cl defect taken at negative and positive biases, respectively. The positive-bias image shows four bright spots at the next-nearest-neighbour (NNN) Cu sites around the defect. (c) Schematic topview of the exposed surface showing the missing Cl defect (dark cross) and the NNN Cu sites (orange circles) with enhanced brightness at positive bias. (d,e) Constant current images ($35 \text{ \AA} \times 35 \text{ \AA}$) around a Ca-site defect taken at the same biases as a and b. The most pronounced feature here is the strongly enhanced topographical intensity of the four nearest Cu sites in the negative-bias image. (f) Schematic structure showing the position of the Ca-site defect (dark dot) and the nearest-neighbour Cu sites (orange circles).

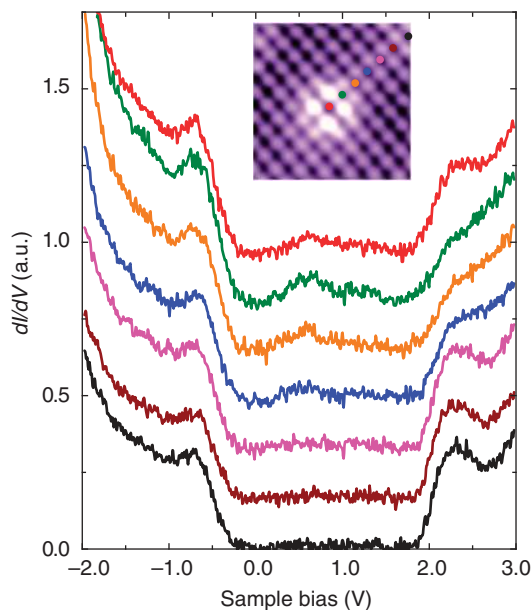


Figure 7 | Spatially resolved electronic structure near the Ca-site defect. dI/dV spectra taken at locations away from the Ca-site defect centre along the Cu-O bond direction, as indicated in the inset image ($35 \text{ \AA} \times 35 \text{ \AA}$) by coloured dots. A broad in-gap state emerges at the defect site. It decays rapidly when moving away from the defect centre and vanishes beyond three lattice sites.

Nevertheless, the electron DOS at E_F is still zero, consistent with an insulating state. The in-gap state intensity drops rapidly with increasing distance from the defect and becomes negligibly small

beyond three lattice constants from the defect centre. Therefore, the in-gap state is also strongly localized in space.

The exact nature of the Ca-site defects is unknown at the current stage, but most likely they donate holes into the Mott insulator. From crystal chemistry point of view, there are two common types of Ca-site defects in CCOC: Ca vacancies due to the high growth temperature and Na substitution of Ca induced by the trace amount of Na impurities during the crystal growth process. Both types of defects are hole donors. The former one donates two holes and the later one donates one hole. CCOC with sufficient amount of Ca vacancies²² or Na dopings²³ have been found to be hole-type superconductors. Furthermore, our STM results show that both the bias dependence of topography and the position of in-gap state on the Ca-site defect are opposite to that of the electron-donor Cl vacancy. As both features are closely related to the doped charge in the Mott insulator, they are also indicative of local hole doping. We note that these are only indirect evidences. To definitively find out the chemical nature of the Ca-site defect, future STM studies on CCOC with controlled amount of Ca vacancies or Na dopants are needed.

Discussion

The properties of parent and lightly doped cuprates are crucial to the mechanism of high T_C superconductivity and have attracted tremendous theoretical interests². It was first proposed by Anderson that the essential physics is contained in the half-filled Hubbard model¹:

$$H = -t \sum_{\langle i,j \rangle \sigma} c_{i\sigma}^{\dagger} c_{j\sigma} + U \sum_i n_{i\uparrow} n_{i\downarrow}$$

Here, t is the hopping integral between nearest-neighbour sites and U is the onsite Coulomb repulsion. In the large U limit as in

the cuprates, the Hubbard model is transformed into the t - J model, where $J = 4t^2/U$ is the superexchange energy. As the two-dimensional Hubbard or t - J models have yet to be solved exactly, various approximation schemes or numerical methods have been employed. The STM results shown here provide unprecedented real-space information and full electronic spectrum that can help discriminate the different models.

A major theoretical debate is whether a single-band model is a valid low-energy model for the cuprates²⁴. The charge transfer nature of the parent insulator suggests that a three band model involving two O bands and one Cu band might be more appropriate. However, it was proposed that the lowest hole-doped state, namely the CTB, can be represented by a single ZRS band²⁵, in which the doped hole residing resonantly in the four planar O sites form a singlet with the central Cu^{2+} ion. There are two specific predictions in the ZRS picture. First, the Mott insulator phase has particle–hole symmetry and second, the ZRS can move freely through the Cu^{2+} lattice and thus should distribute uniformly in space. Our STM results show that undoped CCOC indeed has a nearly particle–hole symmetric and spatially uniform electronic structure, apparently supporting the single-band ZRS model. More quantitatively, the bandwidth of the CTB and UHB estimated from the Gaussian fit is in the order of $3J$ ($J = 0.13$ eV in cuprate), which is also consistent with the calculation based on the single-band t - J model²⁶.

The electronic state induced by a doped charge has also been investigated extensively by theory²⁷. A key issue here is whether the main effect of charge doping is the shift of E_F or the emergence of new states or both. In both the missing Cl and Ca-site defects in CCOC, our STM results demonstrate that a new electronic state is always induced within the charge transfer gap, whereas the position of the Fermi level remains nearly unchanged. We next present a more careful examination of the doped electronic state. In the well-defined missing Cl defect, we find that the doped electron induces an in-gap state near the upper gap edge with its spectral weight mainly transferred from the UHB. The CTB has negligible contribution to the spectral weight transfer. This is inconsistent with the existing theory for electron-doped charge transfer insulators, in which both the CTB and UHB are expected to transfer spectral weight to the in-gap state²⁸. We note that the electron donated by a surface defect studied here may not be an ideal situation owing to the change of local bonding situation and the existence of a defect potential, which may affect both the electronic spectrum and its spatial distributions. The quantitative explanation of these features may require a more sophisticated theoretical treatment like that for the impurity state in superconducting cuprates²⁹. For the Ca-site defect, the in-gap state lies near the lower gap edge with vanishing DOS at E_F . These features are in rough agreement with the calculated DOS for Mott insulator doped with few holes³⁰. As the nature of the defect is still unknown, we will not elaborate on the theoretical implications of the STM results on the Ca-site defect.

Another highly controversial issue regarding doped Mott insulator is whether a doped charge behaves like a coherent quasiparticle. Our STM results on both types of defects demonstrate that the in-gap state has a broad energy distribution and is strongly localized in space. Both features suggest that the doped charge does not behave like a coherent quasiparticle, presumably owing to the strong correlation effect. Indeed, recent theoretical studies show that a single charge doped into the AF Mott insulator is self-localized with vanishing quasiparticle weight^{31,32}.

The atomic-scale STM studies reported here demonstrate that the gross features of the electronic structure of pristine CCOC are consistent with the ZRS model. Although the quantitative in-gap state spectrum and its peculiar spatial variations cannot be

explained readily by existing theory, we show that the emergence of a spatially localized in-gap state is generic for doped Mott insulators. In particular, the surface electron–donor defect represents a well-defined benchmark problem for testing the validity of various many body theories for doped Mott insulators. More importantly, our experiments establish a solid starting point for tackling the high T_C problem. The obvious next step is to apply the atomic-scale large-bias spectroscopy to cuprates with increased dopings, which may elucidate how the Mottness eventually leads to high T_C superconductivity.

Methods

Sample growth. The single crystals of $\text{Ca}_2\text{CuO}_2\text{Cl}_2$ (CCOC) are grown by the flux method as described elsewhere²³. The powders of CaO and CuCl_2 are mixed with a molar ratio of 2:1 and put into an alumina crucible. The mixed powder is heated at 1,053 K for 24 h with intermediate grindings. After that, the CCOC precursor is heated to 1,053 K at a ramp rate of 60 K h^{-1} and kept at this temperature for 5 h. It is then heated to 1,203 K at a ramp rate of 60 K h^{-1} and kept at that temperature for 10 h. In the end, it is cooled down to room temperature at a ramp rate of 60 K h^{-1} . Single crystals with typical size of $2\text{ mm} \times 2\text{ mm} \times 0.1\text{ mm}$ can be harvested by cleaving the as-grown bulks.

STM measurements. The STM experiments are performed with a cryogenic variable temperature ultrahigh vacuum STM system. The CCOC crystal is cleaved *in situ* at $T = 77\text{ K}$ and then transferred immediately into the STM sample stage. To make tunnelling into the insulating CCOC possible, the STM experiments have to be performed at relative high temperature so that the sample has finite conductivity. At $T = 5\text{ K}$, the STM tip will crash into the sample because the sample is so insulating that no tunnelling current can be detected. Therefore, all STM results reported in this paper are acquired at $T = 77\text{ K}$. In addition to that, the sample bias voltage has to be set beyond the charge transfer gap so that there is finite DOS in the sample. The typical setup parameters are sample bias $V_s = \pm 3\text{ V}$ and tunnelling current $I_t = 2\text{--}10\text{ pA}$. The STM topography is taken in the constant current mode, and the dI/dV spectra on CCOC are collected using a standard lock-in technique with modulation frequency $f = 423\text{ Hz}$.

To ensure the reliability of our high-energy tunnelling spectroscopy, we have developed a routine for STM tip treatment and calibration. The tip has to be stable under high biases, and its electronic DOS should be relatively featureless over a wide energy window. We use electrochemically etched polycrystalline tungsten tip for all the measurement. Before the STM experiments on CCOC, the tip is first treated by *in situ* high voltage e-beam sputtering, which is very efficient for cleaning and sharpening the tip. We then use the tip to approach an atomically clean crystalline Au(111) surface prepared *in situ* by repeated Ne ion sputtering and high temperature annealing. By taking topographical scans and spectroscopic measurements on clean Au(111) surface, we could check if the tip shape and spectrum are ideal. If necessary, further tip treatment can be done by field emission process or controlled gentle crash into the Au(111) crystal. Typical calibration data are shown in Supplementary Fig. S1, where both the topography and spectroscopy indicate that the tip is clean and stable. High-quality large-bias, high temperature STM results can usually be obtained with such a tungsten tip.

References

- Anderson, P. W. The resonating valence bond state in La_2CuO_4 and superconductivity. *Science* **235**, 1196–1198 (1987).
- Lee, P. A., Nagaosa, N. & Wen, X. -G. Doping a Mott insulator: physics of high-temperature superconductivity. *Rev. Mod. Phys.* **78**, 17 (2006).
- Waku, K. *et al.* Charge dynamics of $\text{Ca}_{2-x}\text{Na}_x\text{CuO}_2\text{Cl}_2$ as a correlated electron system with the ideal tetragonal lattice. *Phys. Rev. B* **70**, 134501 (2006).
- Abbamonte, P. *et al.* Resonant inelastic X-ray scattering from valence excitations in insulating copper oxides. *Phys. Rev. Lett.* **83**, 860 (1999).
- Hasan, M. Z. *et al.* Electronic structure of Mott insulators studied by inelastic X-ray scattering. *Science* **288**, 1811–1814 (2000).
- Poethuizen, J. J. M. *et al.* Single hole dynamics in the CuO_2 plane at half filling. *Phys. Rev. Lett.* **78**, 717 (1997).
- Ronning, F. *et al.* Photoemission evidence for a remnant Fermi surface and a d-wave-like dispersion in insulating $\text{Ca}_2\text{CuO}_2\text{Cl}_2$. *Science* **282**, 2067–2072 (1998).
- Pan, S. H. *et al.* Imaging the effects of individual zinc impurity atoms on superconductivity in $\text{Bi}_2\text{Sr}_2\text{CaCu}_2\text{O}_{8+\delta}$. *Nature* **403**, 746–750 (2000).
- Hudson, E. W. *et al.* Interplay of magnetism and high- T_c superconductivity at individual Ni impurity atoms in $\text{Bi}_2\text{Sr}_2\text{CaCu}_2\text{O}_{8+\delta}$. *Nature* **411**, 920–924 (2001).
- Hoffman, J. E. *et al.* A four unit cell periodic pattern of quasi-particle states surrounding vortex cores in $\text{Bi}_2\text{Sr}_2\text{CaCu}_2\text{O}_{8+\delta}$. *Science* **295**, 466–469 (2002).

11. Howald, C., Eisaki, H., Kaneko, N., Greven, M. & Kapitulnik, A. Periodic density-of-states modulations in superconducting $\text{Bi}_2\text{Sr}_2\text{CaCu}_2\text{O}_{8+\delta}$. *Phys. Rev. B* **67**, 014533 (2003).
12. Vershinin, M. *et al.* Local ordering in the pseudogap state of the high-Tc superconductor $\text{Bi}_2\text{Sr}_2\text{CaCu}_2\text{O}_{8+\delta}$. *Science* **303**, 1995–1998 (2004).
13. Hanaguri, T. *et al.* A ‘checkerboard’ electronic crystal state in lightly hole-doped $\text{Ca}_{2-x}\text{Na}_x\text{CuO}_2\text{Cl}_2$. *Nature* **430**, 1001–1005 (2004).
14. Gomes, K. K. *et al.* Visualizing pair formation on the atomic scale in the high-Tc superconductor $\text{Bi}_2\text{Sr}_2\text{CaCu}_2\text{O}_{8+\delta}$. *Nature* **447**, 569–572 (2007).
15. Lee, J. *et al.* Spectroscopic fingerprint of phase-incoherent superconductivity in the underdoped $\text{Bi}_2\text{Sr}_2\text{CaCu}_2\text{O}_{8+\delta}$. *Science* **325**, 1099–1103 (2009).
16. Kohsaka, Y. *et al.* Imaging nanoscale electronic inhomogeneity in the lightly doped Mott insulator $\text{Ca}_{2-x}\text{Na}_x\text{CuO}_2\text{Cl}_2$. *Phys. Rev. Lett.* **93**, 097004 (2004).
17. Kohsaka, Y. *et al.* An intrinsic bond-centered electronic glass with unidirectional domains in underdoped cuprates. *Science* **315**, 1380–1385 (2007).
18. Kohsaka, Y. *et al.* Visualization of the emergence of the pseudogap state and the evolution to superconductivity in a lightly hole-doped Mott insulator. *Nat. Phys.* **8**, 534–538 (2012).
19. Shen, K. M. *et al.* Missing quasiparticles and the chemical potential puzzle in the doping evolution of the cuprate superconductors. *Phys. Rev. Lett.* **93**, 267002 (2004).
20. Zaanen, J., Sawatzky, G. A. & Allen, J. W. Band gaps and electronic structure of transition-metal compounds. *Phys. Rev. Lett.* **55**, 418 (1985).
21. Lau, B., Berciu, M. & Sawatzky, G. A. High-spin polaron in lightly doped CuO_2 planes. *Phys. Rev. Lett.* **106**, 036401 (2011).
22. Yamada, I. *et al.* Single-layer oxychloride superconductor $\text{Ca}_{2-x}\text{CuO}_2\text{Cl}_2$ with A-site cation deficiency. *Phys. Rev. B* **72**, 224503 (2005).
23. Hiroi, Z., Kobayashi, N. & Takano, M. Probable hole-doped superconductivity without apical oxygens in $(\text{Ca}, \text{Na})_2\text{CuO}_2\text{Cl}_2$. *Nature* **371**, 139–141 (1994).
24. Phillips, P. & Jarrell, M. Comment on ‘X-ray absorption spectra reveal the inapplicability of the single-band Hubbard model to overdoped cuprate superconductors’. *Phys. Rev. Lett.* **105**, 199701 (2010).
25. Zhang, F. C. & Rice, T. M. Effective Hamiltonian for the superconducting Cu oxides. *Phys. Rev. B* **37**, 3759 (1988).
26. Liu, Z. & Manousakis, E. Dynamical properties of a hole in a Heisenberg antiferromagnet. *Phys. Rev. B* **45**, 2425 (1992).
27. Phillips, P. Colloquium: identifying the propagating charge modes in doped Mott insulators. *Rev. Mod. Phys.* **82**, 1719–1742 (2010).
28. Kusunose, H. & Rice, T. M. Single-particle spectrum in the electron-doped cuprates. *Phys. Rev. Lett.* **91**, 186407 (2003).
29. Balatsky, A. V., Vekhter, I. & Zhu, J. X. Impurity-induced states in conventional and unconventional superconductors. *Rev. Mod. Phys.* **78**, 373–433 (2006).
30. Choy, T. -P. & Phillips, P. Doped Mott insulators are insulators: hole localization in the cuprates. *Phys. Rev. Lett.* **95**, 1–4 (2005).
31. Zhu, Z., Jiang, H. C., Qi, Y., Tian, C. S. & Weng, Z. Y. Self-localization of a single hole in Mott antiferromagnets. Preprint at <http://arXiv.org/abs/1205.5277> (2012).
32. Ye, P. & Wang, Q. R. Strong charge localization in t-J model: non-perturbative monopole effect. Preprint at <http://arXiv.org/abs/1206.0258> (2012).

Acknowledgements

We thank Z.Y. Weng, T. Xiang, F.C. Zhang and G.M. Zhang for helpful discussions. This work is supported by the NSF of China and by the MOST of China (Grants No. 2009CB929402, No. 2010CB923003 and No. 2011CBA00101).

Author contributions

C.Y., P.C., X.Z. and W.R. carried out the STM experiments. R.Y., Q.L. and C.J. grew the CCOC single crystals. Y.W. designed the project and prepared the manuscript. All authors have read and approved the final version of the manuscript.

Additional information

Supplementary Information accompanies this paper at <http://www.nature.com/naturecommunications>

Competing financial interests: The authors declare no competing financial interests.

Reprints and permission information is available online at <http://npg.nature.com/reprintsandpermissions/>

How to cite this article: Ye, C. *et al.* Visualizing the atomic-scale electronic structure of the $\text{Ca}_2\text{CuO}_2\text{Cl}_2$ Mott insulator. *Nat. Commun.* **4**:1365 doi: 10.1038/ncomms2369 (2013).